

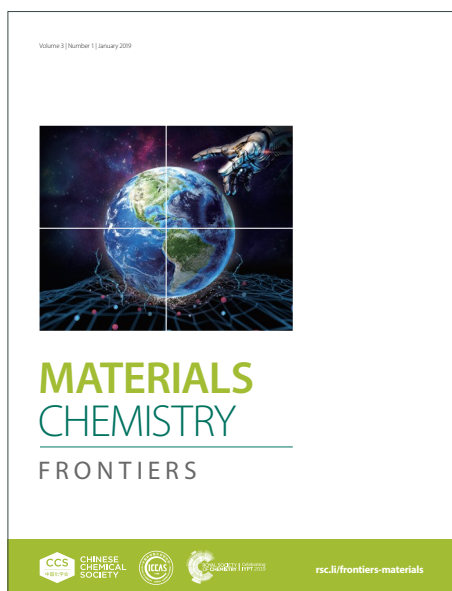
MATERIALS CHEMISTRY

FRONTIERS

Accepted Manuscript



This article can be cited before page numbers have been issued, to do this please use: F. J. Patiño Rodrigo, L. Sánchez-Beato, A. Jiménez, M. Duran, J. L. Polo, I. Payo Gutierrez, J. P. Andres, M. A. Herrero and E. Vázquez, *Mater. Chem. Front.*, 2026, DOI: 10.1039/D6QM00189K.



This is an Accepted Manuscript, which has been through the Royal Society of Chemistry peer review process and has been accepted for publication.

Accepted Manuscripts are published online shortly after acceptance, before technical editing, formatting and proof reading. Using this free service, authors can make their results available to the community, in citable form, before we publish the edited article. We will replace this Accepted Manuscript with the edited and formatted Advance Article as soon as it is available.

You can find more information about Accepted Manuscripts in the [Information for Authors](#).

Please note that technical editing may introduce minor changes to the text and/or graphics, which may alter content. The journal's standard [Terms & Conditions](#) and the [Ethical guidelines](#) still apply. In no event shall the Royal Society of Chemistry be held responsible for any errors or omissions in this Accepted Manuscript or any consequences arising from the use of any information it contains.

ARTICLE

Highly conductive, biocompatible and stretchable sputtered Pt electrode via island-bridge effect

F. Javier Patiño,^{a,b} Lidia Sánchez-Beato,^{a,b} Alicia Jiménez,^{a,b} Mario Durán-Prado,^{c,d,e} J. L. Polo,^f Ismael Payo,^f J.P. Andrés,^g M. Antonia Herrero,^{a,b} * Ester Vázquez.^{a,b} *

Received 00th January 20xx,
Accepted 00th January 20xx

DOI: 10.1039/x0xx00000x

The development of stretchable electrodes is crucial for advancing soft electronics, including bio-integrated health systems and wearable devices. In this work, we present a biocompatible and highly conductive stretchable hydrogel electrode, by combining a conductive polymer (PEDOT:PSS) and a thin platinum layer (≈ 150 nm) deposited on top via radio frequency (RF) sputtering. The 2-hydroxyethyl acrylate (2-HEA) hydrogel provides a flexible matrix into which the PEDOT:PSS polymer is incorporated, along with -OH groups that ensure strong adhesion of the metal layer to the hydrogel. The resulting electrode achieves a surface resistivity of $0.8 \Omega \text{ sq}^{-1}$ ($\approx 8 \times 10^6 \text{ S m}^{-1}$) and maintains conductivity even after 500 stretch-relax cycles at 70% strain. Unlike conventional electrodes, it exhibits minimal resistance variation ($R/R_0 \approx 2$) under strain due to a combined "island-bridge" conduction mechanism. Importantly, the electrode preserves its conductivity even after a year of storage under ambient conditions. Additionally, under 40°C and 70%RH for 48h, the resistivity only shows a slight increase, which is recovered once returned to standard conditions. Furthermore, biocompatibility tests confirm the electrode's suitability for skin-contact applications. This novel approach provides a promising solution for next-generation wearable and implantable bioelectronics, offering an optimal balance between high conductivity, mechanical durability, stretchability and biocompatibility.

1. Introduction

The advancement of soft electronics, which includes applications such as soft robotics,¹⁻³ wearable optical sensors,⁴⁻⁶ and bio-integrated health systems,⁷⁻⁹ is often hindered by the challenge of creating electrodes that can seamlessly conform to complex and dynamic surfaces without compromising electrical performance.^{10, 11} The lack of electrodes that can endure substantial mechanical deformations while maintaining consistent functionality remains a critical bottleneck in the field. As a result, research efforts are increasingly focused on overcoming these limitations by developing electrodes that not only exhibit high conductivity ($>10^3 \text{ S m}^{-1}$) and flexibility but also achieve the much more challenging requirement of substantial stretchability ($>20\%$).^{12, 13} Furthermore, bioelectrodes,

electrodes in contact with living beings, possess the additional requirement of biocompatibility.¹⁴⁻¹⁶ While flexibility can be easily achieved by making the material thinner, obtaining materials with a stretchability superior to 1-2% whereas keeping low electrical resistances is much harder. Broadly, three different approaches have been developed to prepare conductors stretchable above 20% of their initial length: Structure-enabled (Figure 1a), thin films (Figure 1b) and composite-based (Figure 1c), as well as many combination of these three.¹⁷

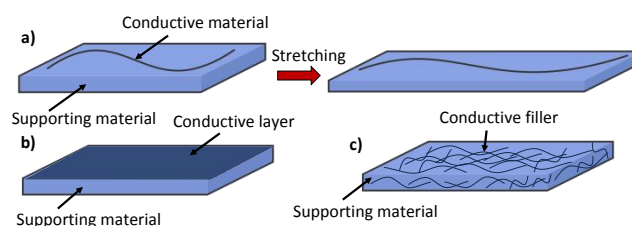


Figure 1. a) Structure enabled scheme. b) Thin films scheme. c) Composite-based scheme.

The structure-enabled procedure takes advantage of the geometrical disposition of conventional materials to allow stretchability. In general, the conductivity of the resulting material can be independent of the strain up to a 50% elongation generally in only one direction, with near-bulk-metal electrical resistance ($\approx 10^7 \text{ S m}^{-1}$).¹⁸ This approach has a maximum strain defined by the geometrical design, further

^a Departamento de Química Inorgánica, Orgánica y Bioquímica, Facultad de Ciencias y Tecnologías Químicas, Universidad de Castilla-La Mancha, 13071 Ciudad Real, Spain.

^b Instituto Regional de Investigación Científica Aplicada (IRICA), UCLM, 13071 Ciudad Real, Spain.

^c Oxidative Stress and Neurodegeneration Group, Medical Sciences Department, Medical School, UCLM, Ciudad Real, Spain.

^d Biomedicine Institute of Castilla-La Mancha, University of Castilla-La Mancha, Ciudad Real, Spain.

^e Instituto de Investigación Sanitaria de Castilla-La Mancha (IDISCAM), Toledo, Spain.

^f School of Industrial and Aerospace Engineering, University of Castilla-La Mancha, Av. Carlos III, 45071 Toledo, Spain.

^g Departamento de Física Aplicada, Instituto Regional de Investigación Científica Aplicada (IRICA), Universidad de Castilla-La Mancha, Ciudad Real, Spain.

Supplementary Information available: [details of any supplementary information available should be included here]. See DOI: 10.1039/x0xx00000x



stretch of the material might lead to irreversible damage and a permanent loss of their conduction.

On the other hand, thin films of metallic material can be deposited over an elastomeric substrate. This approach typically presents a strain-dependent conductivity. Different techniques have been applied to generate those thin films, such as sputtering,¹⁹ screen printing²⁰ or spin coating.²¹ When the elastomer substrate is elongated, the conductor film is stretched and its resistance increases. However, thin-film conductors prepared over elastomers usually degrade with subsequent uniaxial elongations. For example, after several stretch cycles up to 20% of strain, the conductivity of a thin layer of gold deposited on polydimethylsiloxane (PDMS) decreased from $2.8 \cdot 10^6 \text{ S m}^{-1}$ to $\approx 10^4 \text{ S m}^{-1}$.²²

Finally composite-based electrodes are prepared by introducing a conductive filler such as metal nanoparticles, carbon nanotubes or conductive polymers inside an elastomeric structure. This produces intrinsically conductive and stretchable material. As in thin films, the conductivity of the material depends on the elongation. With this method, it is possible to obtain highly elongable conductors (>50%) while maintaining its conductivity.²³ The concentration of the filler is crucial, since filled composites become more brittle and fracture at a lower strain when compared with the unloaded one. Most used conductive fillers include metallic nanowires,²⁴ nano-carbon materials^{25, 26} and conductive polymers (CPs).^{27, 28}

Among these fillers, metallic nanowires are known for their high conductivity, however they suffer from inherent stability issues and a propensity to oxidize,²⁹ unless noble expensive metals like Au or Pt are used.³⁰ Alternatively, carbon nanostructures have been identified for their enhanced stability and impressive carrier mobilities, though they exhibit a high contact resistance.³¹ Both of these materials, carbon nanostructures, and metallic nanowires, face shared challenges, such as the tendency to aggregate and poor adhesion to polymer substrates.³² CPs, on the other hand, exhibit a different set of characteristics. Their conductivity is derived from a π -conjugated system that combines the conductivity of metals and semiconductors enabling higher tuneability. They also allow a more effective interface with soft polymers, coupled with a generally higher level of biocompatibility.³³ This makes them popular materials for stretchable electronics yet they usually present higher resistivities than other fillers.³⁴ Among CPs, poly(3,4-ethylenedioxythiophene)-poly(styrene sulfonate) (PEDOT:PSS) stands out among the others. A deep review about this material was conducted by Chen *et al.*³⁵ It can be tuned to obtain different charge transport abilities, with excellent optical transparency, good electrochemical stability and a long lifetime. The highest conductivity ever reported in PEDOT:PSS based stretchable materials is $3.1 \cdot 10^5 \text{ S m}^{-1}$.³⁶

In this work, we present a biocompatible stretchable hydrogel-based electrode prepared by a combination of two of the previously described methodologies, with the aim of obtaining the intrinsic stretchability of polymeric materials with the conductivity of a thin metal film. We have used a 2-Hydroxyethyl acrylate (2-HEA) based hydrogel whose hydroxyl groups help to integrate both the CP and the thin metal layer.

PEDOT:PSS was selected as the conductive polymer, due to its superior conductivity, the highest recorded among CP fillers. At the surface of this hydrogel, a thin film ($\approx 150 \text{ nm}$) of metallic platinum is deposited via RF sputtering magnetron. The resulting nanocomposite hydrogel exhibits a surface resistivity of $0.8 \Omega \text{ sq}^{-1}$ ($\approx 8 \cdot 10^6 \text{ Sm}^{-1}$) and a maximum elongation of 90%, with the REDOX stability of the platinum metal. This combination of high conductivity and elongation is among the highest reported to date (see section 2.7). These results are explained with an "island-bridge" mechanism, in which, when platinum is stretched, it breaks forming isolated Pt-islands. PEDOT:PSS chains connect these islands, providing alternative pathways for the electric current. Previous examples of this mechanism include the use of carbon nanotubes³⁷ or Ga eutectics with Ag flakes³⁸ as bridging particles which, as depicted previously, can present aggregation problems, and in case of Ga eutectics and Ag, also oxidation issues. In contrast, PEDOT:PSS offers excellent electrochemical stability, intrinsic deformability and easier integration with the hydrogel matrix, rendering excellent performance in fulfilling the bridging role.

Furthermore, all the elements used in this study, 2-HEA,^{39, 40} PEDOT:PSS^{41, 42} and Pt^{43, 44} have been previously used in bioapplications. Therefore, the developed electrode may pave the way for the advancement of next-generation electrodes that are both highly conductive and deformable, with potential applications in biocompatible and wearable systems.

2. Results and discussion

2.1 Hydrogel support

As mentioned previously, the electrode was prepared by the combination of three elements, each one having an important role in the overall material. The 2-HEA monomer is an excellent building block in the preparation of hydrogels and other flexible and hydrophilic materials.^{45, 46} In this way, the 2-HEA based hydrogel contributes to the flexibility of the system and gives the necessary scaffolding and softness. Additionally, it is known from catalysis studies that hydroxyl groups can be adsorbed over platinum nanoparticles with an energy around 30 kJ mol^{-1} .⁴⁷ This adsorption in our case can improve the adhesion of the platinum layer to the substrate hydrogel. This is a key point of this material, as correct interactions between the conductive

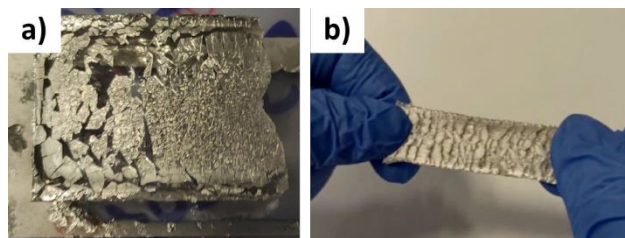


Figure 2: a) Delamination of a platinum thin layer sputtered over an [2-(Acryloyloxy)ethyl]trimethylammonium chloride based hydrogel. b) Conductive silver ink over 2-HEA hydrogels. Both images depict previous unsuccessful attempts to create stretchable electrodes in our group. These failed efforts were part of the iterative process of refining electrode designs to achieve the desired balance of adhesion, conductivity and flexibility



layer and the support play a critical role in the stretchability. Low adhesion forces can cause the delamination of the conductive layer, and the propagation of breaks (Figure 2a). On the other hand, when the adhesion force is too strong, the conductive layer can separate into isolated islands, losing the conductivity (Figure 2b).⁴⁸

The resulting 2-HEA hydrogel itself is an insulating material, whose conductivity was determined to be $7.00 \pm 0.02 \cdot 10^{-8} \text{ S m}^{-1}$. Efforts were made to prepare an electrode using a Pt-modified 2-HEA hydrogel. After Pt deposition, the surface resistance was measured to be $5 \pm 2 \text{ } \Omega \text{ sq}^{-1}$. However, after a single stretch-relaxation cycle, the surface resistance increased, falling outside the specified range.

Therefore PEDOT:PSS is added as a conductive filler,^{49, 50} significantly reducing the resistance of the support, reaching conductivities of $7 \pm 1 \cdot 10^{-1} \text{ S m}^{-1}$ (check experimental section for measurement details). PEDOT:PSS chains are homogeneously distributed through the 3D hydrogel network and fulfill the role of providing alternative pathways for electrons, connecting the metal in case of formation of isolated islands. Although these islands have not been observed at the macroscale in our material, their presence can not be dismissed at the microscale.

2.2 Sputtered Pt layer

The last component, the platinum layer, provides the highest conductivity element. This layer was prepared by RF sputtering magnetron process, as this technique allows fine control of the layer thickness along with good homogeneity and without degradation of the hydrogel support. Furthermore, the resistance of the platinum metal to corrosion and oxidation ensures long-term stability of the electrode.¹⁹

Sputtering requires vacuum conditions, which poses significant challenges when working with highly hydrated hydrogels. Water within the hydrogel tends to evaporate, complicating pressure reduction, and may freeze, potentially damaging the material due to ice formation. A common approach involves sputtering onto another material before depositing it onto the hydrogel,⁵¹ or conducting the sputtering process in a dry state, followed by rehydration.⁵² These methods can lead to issues such as poor adhesion or rupture of the metallic layer, either

during transfer to the hydrogel or during its swelling. The mismatch between the mechanical properties of the metal and the hydrogel, particularly when the material expands upon hydration, increases the risk of delamination or cracking, compromising the electrode's functionality and durability in practical applications. In our case, the 2-HEA hydrogel contains only 5 wt% water, which, even when removed, is regained upon exposure to ambient humidity. This suggests that water interacts sufficiently with the hydrogel to remain inside during sputtering, thereby preventing the previously mentioned issues of evaporation, freezing, and material damage.

Given the challenges previously described and associated with sputtering on water-containing samples, there is limited research on optimal deposition conditions. To address this, different source powers and durations were applied to the 2-HEA/PEDOT support during RF sputtering magnetron, followed by a measurement in the surface resistivity (see section 2.5 for electrical evaluation) to find the optimal conditions. In all cases, the argon pressure was maintained at $1 \cdot 10^{-2}$ torr, and the pre-vacuum was set at $1 \cdot 10^{-4}$ torr. These parameters were crucial for achieving efficient metal deposition without damaging the hydrogel substrate.

First, different power levels (25-250W) were tested while keeping the deposition time constant at 5 minutes. The results (Figure 3a) show that the lowest resistance values were obtained using 100W. For high sputtering powers, the energy of the Pt clusters can damage the substrate.⁵³ For our 2-HEA/PEDOT:PSS hydrogel, this translated to mass losses of up to 15%, 45%, and 98% observed at 150W, 200W, and 250W, respectively. Consequently, higher power leads to excessive damage to the 2-HEA/PEDOT:PSS support. At lower powers, the substrate remained unaltered, making 100W the optimal setting for deposition.

Next, the deposition time was varied while keeping the power constant at 100W (Figure 3b). Initially, surface resistance decreases with time. However, after 5 minutes it increases again. This most likely happens because of overgrowth of the platinum layer, which led to delamination and lower adhesion to the support. Furthermore, longer sputtering times resulted in reduced material stretchability, ultimately leading to the

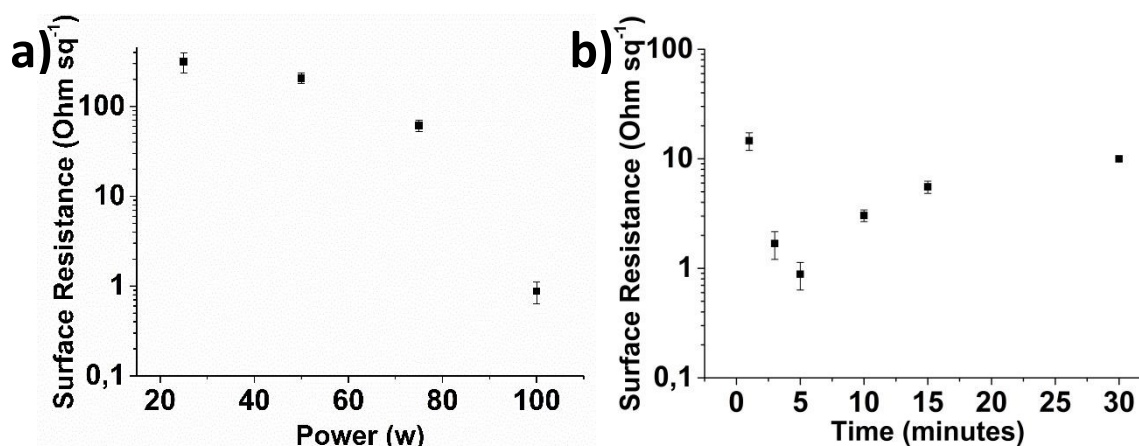


Figure 3: Surface resistivity at a) different powers and b) different time depositions



sample sputtered for 30 minutes becoming completely rigid (see video SM1 in the supporting information). Therefore, the optimal conditions for platinum deposition were established at 100W power, with an argon pressure of $1 \cdot 10^{-2}$ torr and a pre-vacuum of $1 \cdot 10^{-4}$ torr for 5 minutes. These parameters provided the best results for achieving a conductive platinum layer without delamination.

Concerns on the economic viability of the material might arise due to the use of Pt. While Pt is clearly expensive, the quantity used to prepare our material is minimal. Considering our 150 nm thick layer (see section 2.4), preparing 1 m² of electrode requires just 3.2 grams of the metal.

2.3 Mechanical properties

Tensile tests were performed to evaluate the mechanical properties of the material before and after platinum deposition. Representative stress-strain curves (Figure 4) show ultimate tensile strength (UTS) values of 610 ± 90 kPa without platinum and 1600 ± 100 kPa with platinum. The strain to failure (STF) decreased from $260 \pm 30\%$ to $90 \pm 20\%$, and fracture toughness changed from 900 ± 200 kJ m⁻³ to 700 ± 100 kJ m⁻³. These results demonstrate that the sputtering process increased the material's stiffness, though it still retains characteristics of a soft, deformable material. Regarding stretchability, the strain values are similar to other stretchable electrodes presented recently in the literature, which usually present stretchability values between 20-150%.^{20, 54-58}

2.4 Surface Analysis

Representative SEM images of a hydrogel containing only 2-HEA (Figure 5a), 2-HEA/PEDOT:PSS hydrogel (Figure 5b) and 2-HEA/PEDOT:PSS/Pt hydrogel (Figure 5c and 5d) were taken. In these images the 2-HEA hydrogels exhibit a smooth surface with some dust particles also visible. Once the PEDOT:PSS is introduced into the polymeric network, some roughness appears. The emergence of clear dots can be observed in the

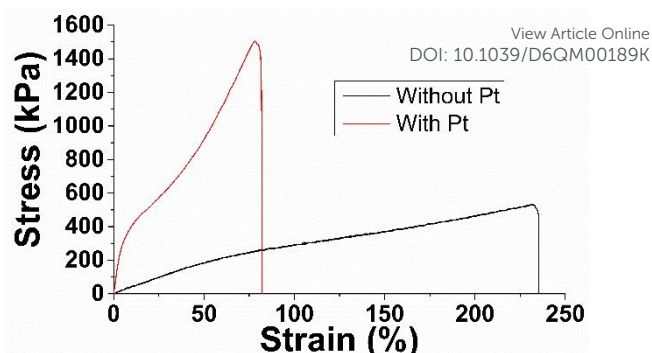


Figure 4: Tensile performance of the stretchable materials before and after platinum deposition.

image, which might correspond to the PEDOT:PSS polymer. When the hydrogel is platinum coated, a continuous layer can be observed, perfectly covering the hydrogel surface. The thickness of this layer can be measured in some fractures present in the material, showing that this layer exhibits 150 ± 30 nm of thickness.

To confirm the uniformity of the platinum deposition, X-ray photoelectron spectroscopy (XPS) analysis was conducted. Samples of 2-HEA/PEDOT:PSS and 2-HEA/PEDOT:PSS/Pt were examined. As shown in Figure 5e, in the absence of platinum, distinct signals corresponding to carbon and oxygen from the hydrogel are observed, along with sulphur signals attributed to the PEDOT:PSS chains. In contrast, upon platinum deposition, these signals are nearly gone, and all Pt signals are visible, masking the underlying elements. This result confirms the homogeneity of the deposition, demonstrating that platinum uniformly covers the hydrogel surface without leaving exposed areas. The XPS signals for O1s, S2s and Pt4f have also been studied. Unfortunately, once the hydrogel is covered, the signals from the sulphur atom disappear completely, and the O1s (≈ 532 eV) is partially overlap by Pt 4p 3/2 (≈ 520 eV). Although this analysis is not clear, the O1s signal seems to be in the same position after the sputtering process (Figure S1), suggesting no clear interaction between Pt and oxygen.

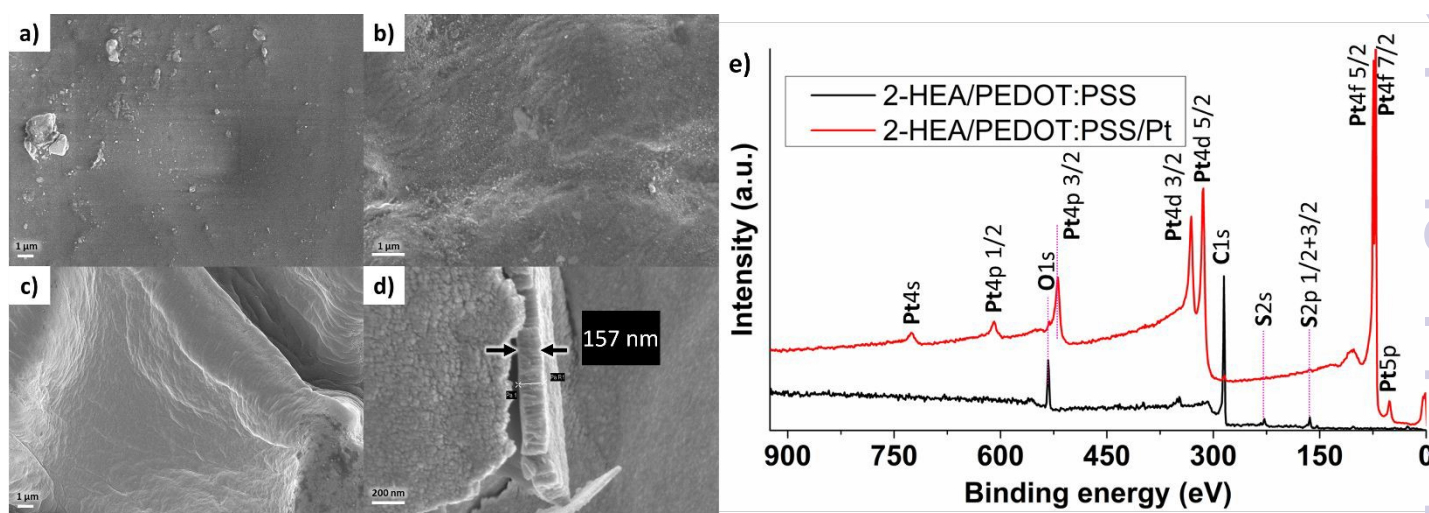


Figure 5: Representative SEM images. a) 2-HEA hydrogel. b) 2-HEA/PEDOT:PSS hydrogel. c) 2-HEA/PEDOT:PSS/Pt sputtered. d) Fracture of a 2-HEA/PEDOT:PSS/Pt sputtered electrode which allows to observe the thickness of the platinum layer. e) XPS spectra of 2-HEA-PEDOT:PSS and 2-HEA-PEDOT:PSS-Pt. The signal without Pt has been amplified (x10) to be comparable with the signal of Pt.



Regarding the Pt4f, the peak was analysed and its signal deconvoluted (Figure S2). Three chemically distinct Pt species were identified:⁵⁹⁻⁶²

- The first doublet, centred at 71.30 eV (4f 7/2) and 74.63 eV (4f 5/2), is assigned to metallic platinum (Pt⁰). These binding energies are in excellent agreement with values for metallic Pt ($\approx 71.0\text{--}71.3$ eV for Pt 4f 7/2).
- A second doublet at 72.11 eV and 75.35 eV is shifted by approximately +0.8 eV relative to Pt⁰. This shift is characteristic of Pt²⁺ species, commonly attributed to PtO or partially oxidized Pt at the surface. Such oxidation is expected for sputtered Pt films after exposure to air, particularly in contact with oxygen-containing substrates.
- The third component, located at 75.27 eV (with the corresponding 4f 5/2 contribution at 79.35 eV), appears at significantly higher binding energy and is consistent with Pt⁴⁺ species, typically assigned to PtO₂. The presence of this higher oxidation state is reasonable considering that thin Pt films can undergo surface oxidation under ambient conditions, especially in humid and oxygen-rich environments such as a hydrogel-based substrate.

Importantly, the observed chemical shifts are fully consistent with well-known platinum oxidation states (Pt⁰, Pt²⁺, and Pt⁴⁺). The binding energy positions do not suggest the formation of specific organometallic Pt–polymer bonds, which would typically produce smaller interfacial shifts rather than the larger displacement observed for the highest binding energy component.

It should be noted that the apparent discrepancy between the O1s and Pt 4f regions is not contradictory. The O1s signal is dominated by the bulk polymer contribution and partially overlaps with the Pt 4p 3/2 level, which limits its sensitivity to subtle interfacial interactions. In contrast, the Pt 4f core level is highly sensitive to the chemical state of platinum and readily reflects surface oxidation.

Additionally, X-Ray Diffraction (XRD) measurements were taken to confirm the crystal structure of the prepared layer. XRD shows peaks at 40.00, 46.45, 67.65, 81.31 and 85.80, corresponding to the reflections (111), (200), (220), (311) and (222), respectively (Figure S3). These peaks are consistent with the face centred cubic (fcc) structure of metallic platinum.⁶³

Furthermore, Attenuated Total Reflectance Fourier Transform Infrared (ATR-FTIR) spectroscopy was used to study the differences before and after the sputtering. Figure S4 shows no significant differences between both materials. Minor differences observed after Pt deposition include a general attenuation of band intensities and slight variations in the 2950–2850 cm⁻¹ (C–H stretching) and 3600–3000 cm⁻¹ (O–H stretching) regions. These changes are attributed to the presence of the continuous metallic Pt layer, which reduces the effective IR penetration depth, and to partial surface dehydration or rearrangement of hydrogen bonding induced by vacuum and plasma exposure during sputtering.

Overall, the XPS, XRD and ATR-FTIR results indicate that Pt deposition does not induce detectable chemical modification of either the hydrogel network or PEDOT:PSS, and that the

interaction between Pt and the polymeric system is predominantly physical and interfacial in nature.

2.5 Electrical properties

The sheet resistance of our 150 nm platinum layer was measured with the four-probe test.⁶⁴ Using this method, it was determined that the pristine material (the never stretched electrode) presents a sheet resistance of $0.8 \pm 0.2 \text{ } \Omega \text{ sq}^{-1}$. Following Equation 1 that correlates the sheet resistance (R_s) with the resistivity (ρ):⁶⁵

$$\rho(\Omega m) = R_s(\Omega/\text{sq}) \cdot t(m) \quad \text{Equation 1.}$$

Where t is the thickness of the conductive material, in our case 150 nm. Therefore, our platinum layer presents a resistivity value of $1.32 \cdot 10^{-7} \text{ } \Omega \text{ m}$. Thus, the conductivity (σ), the inverse of resistivity, for the platinum layer in our material is $8 \pm 3 \cdot 10^6 \text{ S m}^{-1}$, while the conductivity of bulk platinum found in the literature is $9.43 \cdot 10^6 \text{ S m}^{-1}$.⁶⁶ This means that an almost perfect continuous platinum layer has been successfully deposited with practically no defects.

However, the pristine conductivity of the material is not particularly useful for the practical application of a stretchable electrode. Instead, it is more relevant to examine how the material's conductivity evolves during repeated stretch-relax cycles. For this reason, several electrodes were subjected to 70% strain in 500 of these cycles, with surface resistance measured periodically throughout the process (Figure 6). The results demonstrate that after the first cycle, the surface resistance increases substantially, reaching $(6 \pm 3) \text{ } \Omega \text{ sq}^{-1}$ ($\approx 1 \cdot 10^6 \text{ S m}^{-1}$). Following this initial rise, the resistance is maintained approximately constant for up to 500 cycles. The evolution of the tensile curve has been also monitored, showing no considerable fatigue until approaching 500 cycles (Figure S5)

To understand these differences, SEM images of pristine and stretched samples were taken. In the pristine image, it can be observed a uniform, wavy, platinum layer (Figure 7a). However, when looking at the image of the stretched hydrogel, the

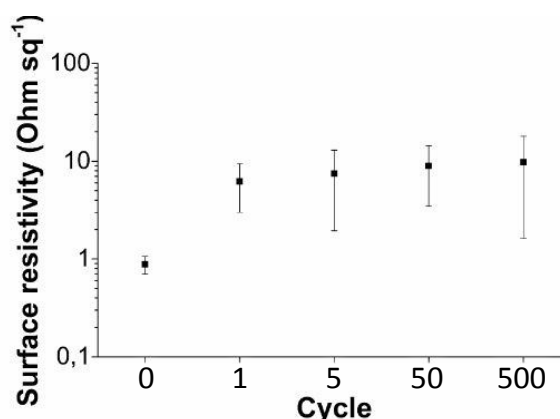


Figure 6: Evolution in surface resistance with several cycles of stretching to 70% strain



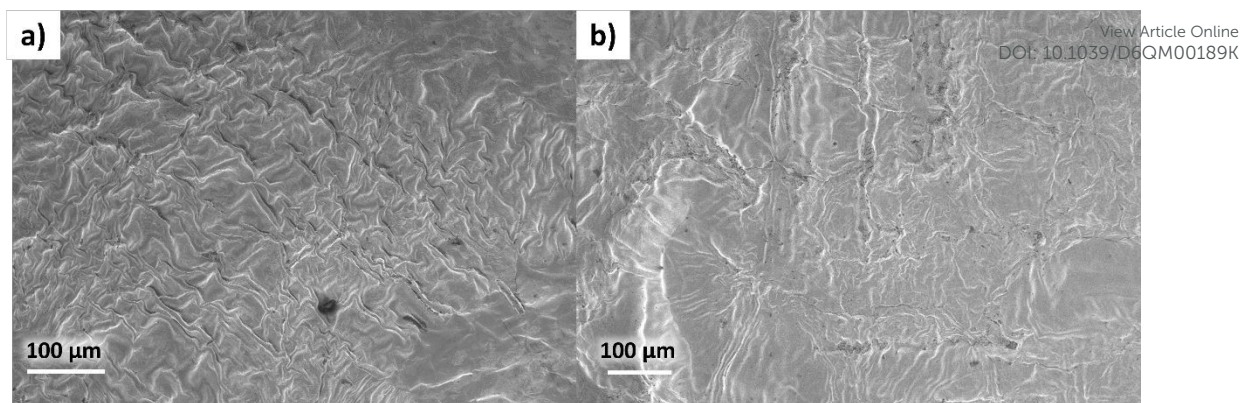


Figure 7: SEM images of a) Pristine electrode and b) stretched electrode.

waviness of the electrode is substantially reduced (Figure 7b). It is possible that this wavy structure formed at the microscale assists our electrode to withstand deformations as it has been previously described in other studies.⁶⁷ During stretching, the polymer chains reorganize and align, reducing the material's waviness. This structural rearrangement may alter the connectivity between PEDOT and Pt, leading to a slight decrease in conductivity. However, once the chains have settled into position, subsequent stretching does not significantly affect the conductivity.

Even after stretching, the conductivity value around $1 \cdot 10^6 \text{ S m}^{-1}$ is one of the highest reported in the literature for this type of electrodes.^{54, 68}

2.5.1 Island-bridge effect

An important parameter for a stretchable electrode is the change in resistance while being stretched. This is precisely

where the island-bridge effect becomes relevant. When the hydrogel is relaxed, the Pt layer remains continuous and in contact throughout, resulting in low resistance. However, upon stretching the electrode, the non-flexible Pt layer fractures and forms small islands. The loss of continuity in the Pt layer is expected to lead to a sharp increase in resistance. Nevertheless, PEDOT:PSS should be able to connect the different islands, limiting the overall rise in resistance (Figure 8a).

In this scenario, PEDOT could act as an alternative pathway for electrons. Although the conductivity of PEDOT:PSS materials typically range between 10 to 10^3 S m^{-1} ,⁶⁹ recent advancements using laser treatments report conductivities up to $9 \cdot 10^4 \text{ S m}^{-1}$,^{70, 71} and crystalline PEDOT has been found to obtain conductivities higher than 10^5 S m^{-1} ,⁷² which would allow an effective island-bridge effect.

To evaluate this behaviour, non-pristine samples (electrodes stretched at least once) were uniaxially stretched,

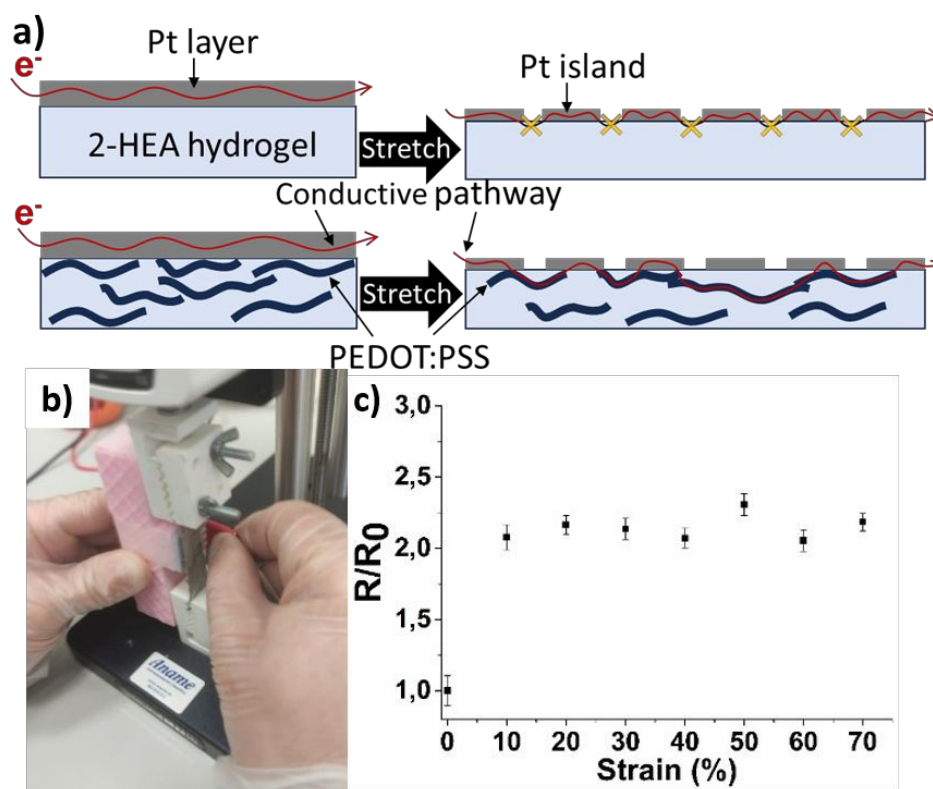


Figure 8: a) Conductivity pathways inside the electrode with and without PEDOT:PSS. b) Picture of the measurement set-up. c) Resistance variations with strain.



and the resistance was recorded using four electrodes (Figure 8b). Importantly, the four-points probes were not attached to the sample during stretching. After each measurement, the probes were removed and then repositioned for the next measurement. This ensures that the distance between the four electrodes remained constant, and that only the deformation of the sample contributed to the resistance change. In Figure 8c, it can be observed that when stretching begins, the resistance doubles but afterwards it remains almost constant for the rest of the actuation.

Typically, resistance progressively increases as the material is stretched, often reaching values several orders of magnitude higher than the initial resistance,^{19, 73-76} entirely different from the stable behaviour observed in this material. This behaviour aligns perfectly with the island-bridge mechanism previously mentioned. Initially, the platinum layer is well-connected, showing lower resistance. When the electrode begins to stretch, the metal layer is broken at the nanoscale, but PEDOT chains are able to keep the connection between them, although at the cost of a slightly higher resistance. Once these bridges are formed, the resistance does not increase further, as PEDOT itself is able to stretch while keeping the platinum islands connected.

In order to follow the formation of those islands, SEM images of the electrode stretched at 20% (Figure 9a) and at 60% (Figure 9b) were taken. These images reveal the formation of cracks in the platinum layer, confirming the formation of the platinum islands described earlier. Cracks form predominantly perpendicular to the direction of the applied tensile strain. At 20% strain, the crack widths are typically in the range of 20 to 30 nm, whereas at 60% strain the number of cracks increases and they become wider, reaching approximately 35 to 60 nm.

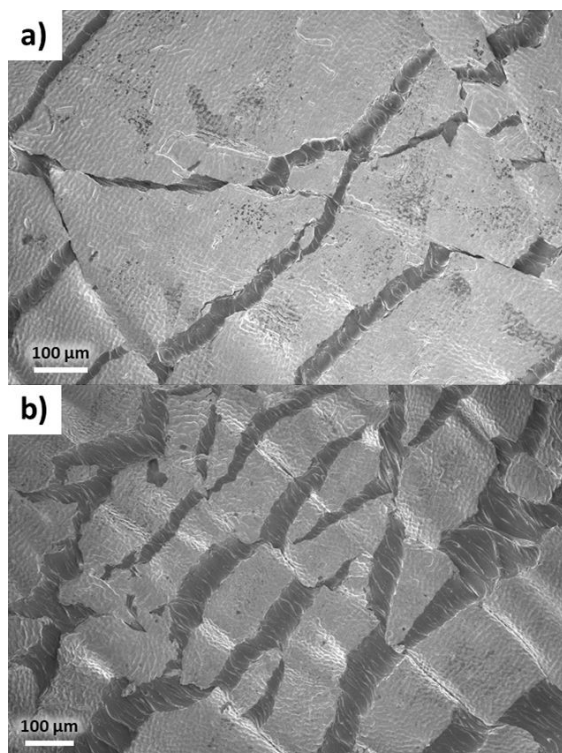


Figure 9: SEM images of an electrode stretched at a) 20% and b) 60%

2.5.2 Stretchable electrode proof of concept.

View Article Online

DOI: 10.1039/D6QM00189K

To illustrate the capabilities of this electrode, in Figure 10, its application for diode illumination is shown. In this configuration, the electrical contacts are fixed at the two ends of the electrode. The hydrogel underwent stretching, twisting, and concurrent deformation, with the light emission consistently sustained. It is worth highlighting that under tensile strain, a discernible reduction in light intensity was observed. Although this may appear to contradict the results shown in Figure 8c, this behaviour is expected because stretching increases the distance between the fixed electric contacts, thereby increasing the overall resistance of the electrode. The electric potential across the circuit was rigorously upheld at 2.5V DC throughout the entirety of the experimentation (see video SM2 in supporting information).

In order to highlight the important role played by PEDOT:PSS in the matrix, a 2-HEA hydrogel without PEDOT:PSS was prepared, and Pt was sputtered on top. The same experiment was performed, but this time when stretched, the LED went out. More importantly, after a few stretching cycles, the LED failed to light even when relaxed (SM3 see video in supporting information).

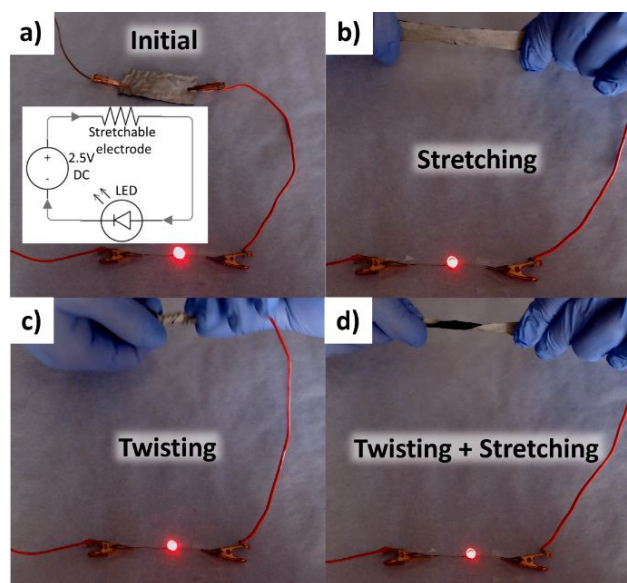


Figure 10: a) Initial state. b) Stretching. c) Twisting. d) Twisting and stretching.

2.5.3 Long term and ambient conditions stability

Another key aspect for stretchable electrodes is their long-term stability under varying ambient conditions. To evaluate this, we analysed the stability of our electrodes in three scenarios: ambient aging, high-humidity/temperature exposure, and water immersion.

First, the long-term stability was assessed by re-measuring non-pristine electrodes prepared over one year ago. These samples were stored in a standard laboratory cabinet, exposed to ambient air (not hermetically sealed). The surface resistance of these aged, non-pristine electrodes was $4 \pm 2 \Omega \text{ sq}^{-1}$. Notably, this value is slightly lower than that of freshly stretched non-



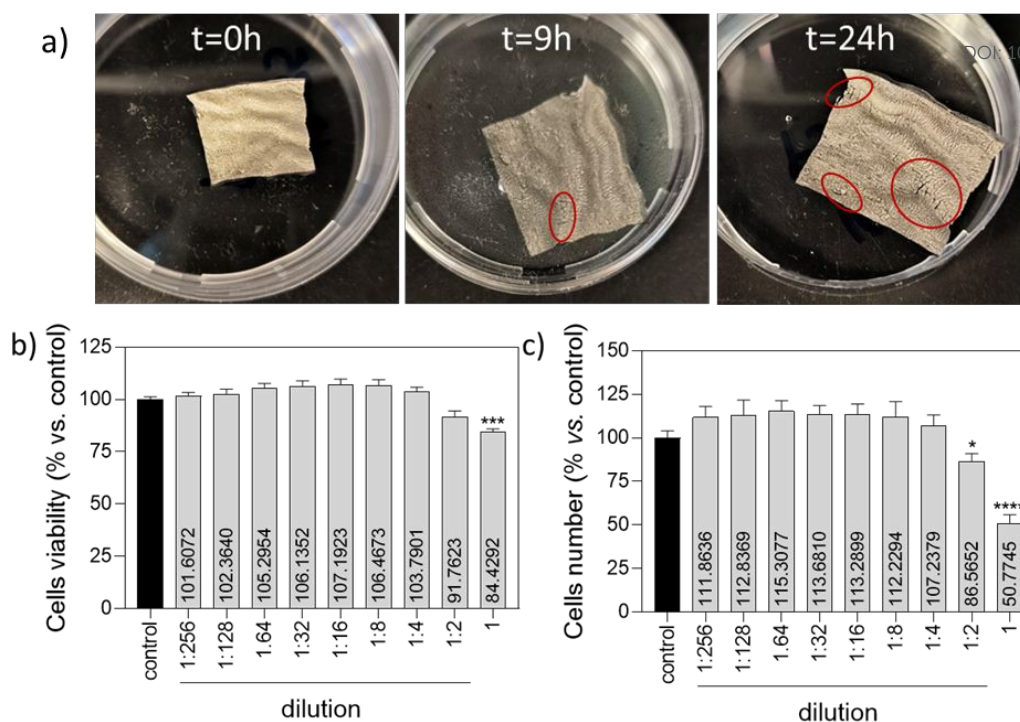


Figure 11: a) Evolution of the electrode when immersed in water. The hydrogel swells and some defects, marked in red, appears. b) Cell viability. c) Cells number. Percentages are given relative to control.

pristine electrodes measured immediately after deformation ($6 \pm 3 \Omega \text{ sq}^{-1}$). This observation suggests that the polymer matrix requires time to fully relax after stretching; as internal stresses dissipate over time, the surface resistance decreases to a stable minimum. This finding highlights the long-term structural stability of the electrode once the material has reached its equilibrium state.

Subsequently, to simulate the vapour phase of sweat or high-humidity environments, the same aged electrodes were placed in a humidity chamber at 70% RH and 40 °C for 48 h. The surface resistance increased to $8 \pm 3 \Omega \text{ sq}^{-1}$. This rise can be attributed to the volume expansion of the hydrogel caused by water absorption, which induces a slight tensile strain on the conductive network, thereby increasing resistance. To verify the reversibility of this effect, the same electrodes were returned to ambient conditions (24 °C, 35% RH) for 30 minutes. The resistance recovered to $6 \pm 2 \Omega \text{ sq}^{-1}$, a value indistinguishable from that of freshly stretched electrodes. This confirms that the resistance change under high humidity is largely reversible and linked to physical swelling, rather than permanent chemical degradation or delamination.

Finally, the electrodes were immersed in water for 24h. Unfortunately, during this time the electrode slowly developed some defects. Importantly, some peel-off of the platinum layer is visible, suggesting that water is interfering with the Pt-OH interaction (Figure 11a).

Collectively, these results demonstrate that while the electrode is vulnerable to liquid immersion, it exhibits robust stability under high-humidity and ambient aging conditions. These conditions are more representative of the vapour phase encountered in real-world skin-contact and wearable

applications, validating the material's suitability for such environments.

2.6 Cell viability test

As described before, the toxicity of PEDOT:PSS, 2-HEA hydrogels and platinum has been studied previously, showing no significant effect on cell viability.³⁹⁻⁴⁴ However, we have found that our electrode tends to slowly degrade when immersed in water for long periods of time, indicating the possibility of releasing potentially toxic compounds. In this extreme scenario, it is crucial to assess whether these compounds may affect the cells or not.

Currently, various methodologies are available to evaluate the biocompatibility of hydrogels, depending on the material's intended application.^{39, 77, 78} In the case of our electrode, its primary application as a stretchable electrode lies in the development of deformable wearable devices, and therefore it is expected to be positioned externally, potentially in contact with the skin.

In addition, the degradation of the material only occurs when immersed in aqueous media. Therefore, the analysis of potential hydrogel extracts is sufficient to determine its applicability.⁴⁰ For this reason, the electrode was immersed in culture medium for 24h, and subsequently used this medium for cell culture experiments with keratinocytes. Results (Figure 11b,c) show that, with a concentration of 100% extracts, the cell viability is 85%, while the cell number is reduced to 50%. However, when the concentration of the extracts decreases to 25%, both the cell number and the cell viability remain unaltered.



These results show that high concentrations of the electrode extracts might have a negative effect on the skin. However, in real-world scenarios, the extracts released would be less concentrated, mainly caused by sweat or other body fluids. These wouldn't be as abundant as in the test and would not come into direct and prolonged contact with the skin, thereby minimizing the risk of cytotoxic effects and allowing its implementation.

2.6 Contextualization within existing literature

Finally, to add more context to our work, a comparison of the properties of our material with other remarkable stretchable electrodes published can be found in Table 1. In that table, we

can see how our material presents one of the best relationships between conductivity and strain (Figure 12). Additionally, when considering the changes in resistance when stretched (R/R_0) our material also highlights among the others. The combination of stretchability, conductivity and changes in resistance while stretching, is only surpassed by liquid metals (EGaIn) electrodes. However, the stability issues of EGaIn alloy are known to be an important limitation of these kinds of electrodes.⁷⁹ Lastly, regarding the biocompatibility of these electrodes, it can be shown that most of them do not study their biocompatibility.

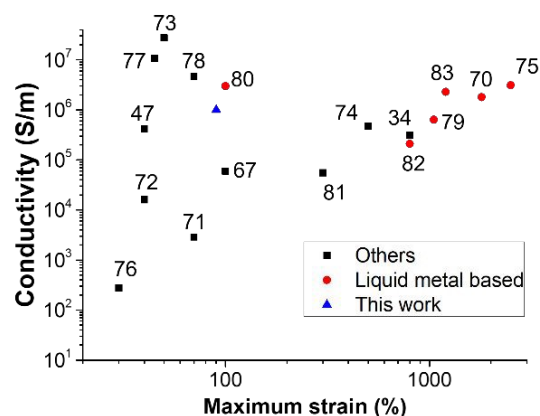


Figure 12: Conductivity and maximum strain of the most remarkable reported electrodes

Reference	Conductive material	Conductivity (S m ⁻¹)	Maximum Stretchability (%)	R/R ₀ at X% strain	Nº of fatigue cycles at X% strain	Biocompatible
25	Carbon nanotubes (CNTs)	6.3	500	1.2 at 70%	25000 at 50%	Not reported
36	PEDOT:PSS	3.1·10 ⁵	800	1 at 100%	1000 at 100%	Not reported
49	Graphene PEDOT:PSS	4.14·10 ⁵	40	200 at 40%	Not reported	Not reported
76	PEDOT:PSS	5.99·10 ⁴	100	2 at 50%	1000 at 100%	Not reported
79	EGaIn	1.8·10 ⁶	1800	1 at 70%	25000 at 100%	Yes



80	Ag nanoparticles (AgNPs)	$2.86 \cdot 10^3$	70	2 at 30%	10000 at 20%	Not reported
81	Ag-PTFE:CNT	$1.61 \cdot 10^4$	40	6 at 40%	1000 at 20%	Not reported
82	Ag nanowires (AgNW) and Gold	$2.75 \cdot 10^7$	50	2 at 30%	1000 at 30%	Not reported
83	AgNW	$4.8 \cdot 10^5$	500	2 at 70%	30000 at 50%	Not reported
84	EGaIn	$3.12 \cdot 10^6$	2500	1.22 at 100%	1500 at 100%	Not reported
85	Ag	$2.76 \cdot 10^2$	30	2.5 at 30%	3000 at 30%	Not reported
86	AuNP	$1.08 \cdot 10^7$	45	10 at 45%	Not reported	Yes
87	AgNW	$4.67 \cdot 10^6$	70	4 at 70%	1000 at 30%	Not reported
88	Ag flakes+ EGaIn	$6.38 \cdot 10^5$	1050	1 at 70%	500 at 100%	Yes
89	EGaIn and CNTs	$3 \cdot 10^6$	100	3 at 70%	10000 at 100%	Not reported
90	Whiskered gold nanosheets	$5.5 \cdot 10^4$	300	3.3 at 50%	200 cycles at 40%	Yes
91	EGaIn and PEDOT:PSS	$2.1 \cdot 10^5$	800	0.8 at 80%	500 cycles at 25%	Not reported
92	EGaIn	$2.3 \cdot 10^6$	1200	1 at 100%	5000 cycles at 100%	Not reported
This work	Pt and PEDOT:PSS	$1 \cdot 10^6$	90	2 at 70%	500 at 70%	Yes

Table 1: Most remarkable stretchable electrodes reported in bibliography.

3. Experimental section

3.1 Materials and reagents

Reagents were used as purchased from commercial sources without further purification. 2-hydroxyethylacrylate (2-HEA) and polyethylene glycol diacrylate (PEGDA, M_n 700) were obtained from Sigma-Aldrich. PEDOT:PSS 1,3% (Clevios, PH1000) dispersion was bought from Heraeus. Lithium 2,4,6-trimethylbenzoylphosphonate photoinitiator was synthesized according to Benedikt et al.⁹³

3.2 Hydrogel fabrication and Pt deposition

In a typical synthesis, the hydrogel was prepared by the polymerization of 4 mL (34 mmol) of the 2-hydroxyethylacrylate (2-HEA) monomer, using 30 mg (≈ 0.04 mmol) of polyethylene glycol diacrylate (PEGDA, M_n 700) as crosslinker agent and 20 mg (0.06 mmol) of lithium 2,4,6-trimethylbenzoylphosphinate (LiTPO) as photoinitiator. 5 mL of an aqueous dispersion of 1,3% of PEDOT:PSS was used as solvent. The polymerization process was done in 3 minutes under UV light ($\lambda=365$ nm), adding 3 mL of the precursor solution over a glass slide to obtain thin films of the 2-HEA/PEDOT:PSS hydrogel ($2.5 \times 7.5 \times 0.2$ cm). The resulting material is a dark-blue, stretchable and slightly conductive hydrogel. Unlike other hydrogels, it remains flexible, without drying at ambient conditions. When exposed to high temperatures in an oven, a 5% of mass (water) loss can be

observed, which is recovered once the hydrogel is back in ambient conditions.

Afterwards, the hydrogel was introduced in a vacuum chamber to perform the sputtering process and deposit the platinum layer over the hydrogel. A Leybold Z400 sputtering machine was used, with a 3-inch Pt target and a Hüttinger RF source. This target size ensures homogeneous deposition across the sample surface, which typically consists of a 2.5×7.5 cm rectangular area. For the sputtering process, an argon pressure of $1 \cdot 10^{-2}$ mbar with a pre-vacuum of $1 \cdot 10^{-4}$ mbar is used. The source power and deposition time were varied according to the experiments, from 25W to 250W and from 1 minute to 30 minutes respectively.

3.3 Hydrogel characterization

Mechanical properties of the hydrogel have been studied through tensile tests using a Mecmesin Multitest 2.5-i dynamic mechanical analyser. Six different hydrogels samples following the ISO-37 standard were anchored by tweezers on the analyser and monoaxially stretched at $50 \text{ mm} \cdot \text{min}^{-1}$ until failure, recording the stress and strain of the material. A cell load of 50N is used in this process. Three parameters can be obtained from this test: ultimate tensile strength (UTS, maximum y-axis coordinate), strain to failure (STF, maximum x-axis coordinate) and fracture toughness (area under the curve).

The morphological structure of the material has been studied using GeminiSEM 500 instrument (Zeiss) scanning electron microscope.



X-ray photoelectron spectroscopy (XPS) spectra were acquired using a FlexPS system from Specs. A monochromatic aluminium anode (1486.71 eV) served as the excitation source, operating at 14 kV and 300 W. All data is referenced to C 284.5 eV. Deconvolution was performed using CasaXPS software. Prior to measurement, samples underwent 10 minutes of argon etching in Fine Beam mode, with an ion energy of 5 kV and an emission current of 10 mA. This procedure ensured the removal of surface contaminants, such as atmospheric CO₂ and H₂O, resulting in a clean sample surface for accurate analysis.

X-ray diffraction (XRD) measurements were carried out using a Bruker D8 Advance diffractometer equipped with 0.6 mm and 1 mm slits. The instrument operates with a Cu radiation source ($\lambda = 1.5428 \text{ \AA}$) at 40 kV and 40 mA. The system is equipped with a Göbel mirror for beam collimation and a LynxEye detector.

FTIR spectra were recorded with a with a Jasco FT/IR-4700 using KBr pellets.

Electrical properties of the material have been studied using a 4 probes test Jandel model RM3000 to obtain the sheet resistance. The measurements of the resistance while stretching have been done with an Autolab/PGSTAT204 impedance meter. To measure the conductivity of the 2-HEA gel without PEDOT:PSS, the two-electrode method was used in combination with an Agilent E4980A LCR impedance meter.

3.4 Diode illumination

The LED illumination application was performed using a HQ power PS3003 power supply, with $\Delta E = 2.5 \text{ V}$ in direct current. The LED and the electrode were connected in series.

3.5 Cell viability test

The prepared electrode was sterilized by immersion in ethanol for 2h followed by another 4h of UV irradiation. Afterwards, the electrode ($\approx 0.3 \text{ g}$) was immersed in 8 mL of DMEM culture medium (Sigma-Aldrich) supplemented with inactivated 10% fetal calf serum, 2 mM L-glutamine, 1 mM sodium pyruvate, 0.1 mg/mL streptomycin and 0.1 mg/mL ampicillin, maintained at 37 °C in 5% CO₂ for 24h. Different concentrations of this culture medium with the hydrogel extracts were used to culture keratinocytes cells (Thermo Fisher) for 48h. For cells viability and related assays, cells were cultured in optical 96-well plates at a density of 1×10^4 cells/well. Cells were loaded with 1 μM calcein-AM (Thermo Fisher Scientific Inc., Waltham, MA, USA), 1 μM propidium iodide (Sigma) and 1 μM Hoechst (Thermo Fisher) for 30 min to assess viability as described previously.⁹⁴ Whole-well fluorescence for green, red and blue channels was recorded by microfluorimetry and well were scanned for each channel with a 20x objective using a Cytation 5 equipment (BioTek, Agilent). Blue fluorescence indicates the total number of cells. Cell viability was calculated from green fluorescence, normalizing to blue fluorescence. Results are expressed as percentage of viable vs. total cells (Fig. 11b), and total cell number (Fig. 11c).

4. Conclusions

A new, highly conductive and stretchable electrode based on a 2-HEA hydrogel with PEDOT:PSS and sputtered Pt has been prepared and characterized. Mechanical properties have been studied via tensile test, determining a deformability of 90 \pm 20%. Electrical characterization has determined the high conductivity of the material ($1 \cdot 10^6 \text{ S m}^{-1}$ after stretching the electrode), and surface characterization studies with SEM, XRD, XPS and FTIR have shown that the platinum forms a uniform, continuous layer of 150 \pm 30 nm thick, even after stretching. The stability of the material to withstand subsequent cycles of stress has been proven together with its long-term stability and harsh ambient conditions resistance. Furthermore, the change in resistance while stretching is remarkably low with $R/R_0 = 2$. Finally, its application as stretchable connector was illustrated, along with its biocompatibility, which allows its applicability in deformable wearables.

Author contributions

F. Javier Patiño: investigation, writing-original draft, writing-review & editing. Lidia Sanchez-Beato: investigation. Alicia Jiménez: Investigation. Mario Durán-Prado: Formal analysis, writing-review & editing. J.L. Polo: Resources, writing-review & editing. Ismael Payo: Resources, writing-review & editing. J.P. Andrés: Resources, writing-review & editing. M. Antonia Herrero: Writing – review & editing, supervision, funding acquisition, conceptualization. Ester Vázquez: Writing – review & editing, supervision, funding acquisition, conceptualization.

Conflicts of interest

There are no conflicts to declare

Data availability

A data availability statement (DAS) is required to be submitted alongside all articles. Please read our full guidance on data availability statements for more details and examples of suitable statements you can use.

Acknowledgements

The authors are grateful for financial support from the Spanish Government (Project PID2023-150894OB-I00), the Junta de Comunidades de Castilla-La Mancha (Project SBPLY/21/180501/000135/1) and University of Castilla-La Mancha (2022-GRIN-34415). This study is part of the Advanced Materials program and was supported by MCIN with funding from the European Union NextGenerationEU (PRTR-C17.I1) and the Junta de Comunidades de Castilla-La Mancha. F. J. Patiño would also like to express his gratitude to Castilla-La Mancha community board for their pre-Ph.D. contract (2020-PREDCLM-16324).



Notes and references

- J. Shintake, S. Rosset, B. Schubert, D. Floreano and H. Shea, Versatile Soft Grippers with Intrinsic Electro-adhesion Based on Multifunctional Polymer Actuators, *Adv. Mater.*, 2016, **28**, 231-238.
- P. A. Zhu, W. Tang, Z. D. Jiao, H. X. Xu, Y. Hu, Y. Qu, H. Y. Yang and J. Zou, Liquid Manipulator with Printed Electrode Patterns for Soft Robotic Systems, *Adv. Mater. Technol.*, 2023, **8**, 2300308.
- Y. Z. Wang, P. P. Zhang, H. Huang and J. Zhu, Bio-Inspired Transparent Soft Jellyfish Robot, *Soft Robot.*, 2023, **10**, 590-600.
- J. Pan, Z. Zhang, C. Jiang, L. Zhang and L. Tong, A multifunctional skin-like wearable optical sensor based on an optical micro-/nanofibre, *Nanoscale*, 2020, **12**, 17538-17544.
- J. Guo, B. Zhou, C. Yang, Q. Dai and L. Kong, Stretchable and upconversion-luminescent polymeric optical sensor for wearable multifunctional sensing, *Opt. Lett.*, 2019, **44**, 5747-5750.
- F. E. Lin and W. L. Cheng, 3D Sponge Electrodes for Soft Wearable Bioelectronics, *Adv. Electron. Mater.*, 2023, **9**, 2300334.
- C. Lou, S. Wang, T. Liang, C. Pang, L. Huang, M. Run and X. Liu, A Graphene-Based Flexible Pressure Sensor with Applications to Plantar Pressure Measurement and Gait Analysis, *Materials*, 2017, **10**, 1068.
- K. Kwon, J. U. Kim, Y. Deng, S. R. Krishnan, J. Choi, H. Jang, K. Lee, C.-J. Su, I. Yoo, Y. Wu, L. Lipschultz, J.-H. Kim, T. S. Chung, D. Wu, Y. Park, T.-i. Kim, R. Ghaffari, S. Lee, Y. Huang and J. A. Rogers, An on-skin platform for wireless monitoring of flow rate, cumulative loss and temperature of sweat in real time, *Nat. Electron.*, 2021, **4**, 302-312.
- M. Namkoong, B. Baskar, L. Singh, H. Guo, J. McMurray, K. Branan, M. S. Rahman, C. T. Hsiao, J. Kuriakose, J. Hernandez, A. A. Arikian, L. E. Garza-Rivera, G. L. Coté and L. M. Tian, Add-On Soft Electronic Interfaces for Continuous Cuffless Blood Pressure Monitoring, *Adv. Mater. Technol.*, 2023, **8**, 2300158.
- N. Cui, Y. Song, C.-H. Tan, K. Zhang, X. Yang, S. Dong, B. Xie and F. Huang, Stretchable transparent electrodes for conformable wearable organic photovoltaic devices, *npj flex. electron.*, 2021, **5**, 31.
- H. Tang, Y. Li, S. Liao, H. Liu, Y. Qiao and J. Zhou, Multifunctional Conductive Hydrogel Interface for Bioelectronic Recording and Stimulation, *Adv. Health. Mater.*, 2024, **13**, 2400562.
- T. Cheng, Y. Zhang, W.-Y. Lai and W. Huang, Stretchable Thin-Film Electrodes for Flexible Electronics with High Deformability and Stretchability, *Adv. Mater.*, 2015, **27**, 3349-3376.
- Y. Kim, O. Y. Kweon, Y. Won and J. H. Oh, Deformable and Stretchable Electrodes for Soft Electronic Devices, *Macromol. Res.*, 2019, **27**, 625-639.
- J. H. Min, J. B. Tu, C. H. Xu, H. Lukas, S. Shin, Y. R. Yang, S. A. Solomon, D. Mukasa and W. Gao, Skin-Interfaced Wearable Sweat Sensors for Precision Medicine, *Chem. Rev.*, 2023, **123**, 5049-5138.
- Y. Lu, Z. Jin, Y. Jian, D. Kong, H. Zhou, Y. Xu, R. Cao, Z. Xia, F. Yang, Q. Wu, Y. Gao, A. Cui, S. Yang, N. Zheng, J. Bang, G. Yang, S. H. Ko, H. Yang and K. Xu, Metal-hydrogel chelation interfaces for ultrasoft and bidirectional bioelectronics, *National Science Review*, 2025, **12**, nwaf399.
- Y. Xu, L. Deng, Y. Lu, J. Zhang, Z. Xu, K. Xu and C. Zhang, Organohydrogel-Based Soft SEMG Electrodes for Algorithm-Assisted Gesture Recognition, *Advanced Sensor Research*, 2024, **3**, 2300164.
- I. M. Graz and S. Rosset, in *Organic Flexible Electronics*, eds. P. Cosseddu and M. Caironi, Woodhead Publishing, 2021, pp. 479-500.
- M. Drack, I. Graz, T. Sekitani, T. Someya, M. Kaltenbrunner and S. Bauer, An Imperceptible Plastic Electronic Wrap, *Adv. Mater.*, 2015, **27**, 34-40.
- H.-M. Sim, Y.-K. Oh, Y. Yu, S. Kim and H.-K. Kim, Super-stretchable polymer-AgPdCu superlattice electrodes for high-performance wearable electronics, *Composites Part B: Engineering*, 2022, **238**, 109914.
- S. Yoon and H.-K. Kim, Cost-effective stretchable Ag nanoparticles electrodes fabrication by screen printing for wearable strain sensors, *Surf. Coat. Technol.*, 2020, **384**, 125308.
- J. Y. Lee, S. Y. Han, Y. C. Nah and J. Park, Fabrication of Stretchable Ag Nanowire Electrode and its Electrochromic Application, *Korean J. Mater. Res.*, 2019, **29**, 87-91.
- I. M. Graz, D. P. J. Cotton and S. P. Lacour, Extended cyclic uniaxial loading of stretchable gold thin-films on elastomeric substrates, *Appl. Phys. Lett.*, 2009, **94**.
- C.-Y. Huang and C.-W. Chiu, Facile Fabrication of a Stretchable and Flexible Nanofiber Carbon Film-Sensing Electrode by Electrospinning and Its Application in Smart Clothing for ECG and EMG Monitoring, *ACS Appl. Electron. Mater.*, 2021, **3**, 676-686.
- Q. Liao, W. Hou, J. Zhang and L. Qin, Controllable Preparation of Silver Nanowires and Its Application in Flexible Stretchable Electrode, *Coatings*, 2022, **12**, 1756.
- X. Gong, Z. Chu, G. Li, Y. Tan, Q. Dong, T. Hu, Z. Zhao and Z. Jiang, Efficient Fabrication of Carbon Nanotube-Based Stretchable Electrodes for Flexible Electronic Devices, *Macromol. Rapid Commun.*, 2023, **44**, 2200795.
- S. Yan, G. Zhang, H. Jiang, F. Li, L. Zhang, Y. Xia, Z. Wang, Y. Wu and H. Li, Highly Stretchable Room-Temperature Self-Healing Conductors Based on Wrinkled Graphene Films for Flexible Electronics, *ACS Appl. Mater. Interfaces*, 2019, **11**, 10736-10744.
- A. Spanu, A. Botter, A. Zedda, G. L. Cerone, A. Bonfiglio and D. Pani, Dynamic Surface Electromyography Using Stretchable Screen-Printed Textile Electrodes, *IEEE Trans. Neural Syst. Rehabil. Eng.*, 2021, **29**, 1661-1668.
- S. Yang, C. Liu, L. Tang, J. Shang, J. Zhang and X. Jiang, Highly Adhesive and Stretchable Epidermal Electrode for Bimodal Recording Patch, *ACS Appl. Mater. Interfaces*, 2024, **16**, 43880-43891.
- J. J. Patil, W. H. Chae, A. Trebach, K.-J. Carter, E. Lee, T. Sanniccolo and J. C. Grossman, Failing Forward: Stability of Transparent Electrodes Based on Metal Nanowire Networks, *Adv. Mater.*, 2021, **33**, 2004356.
- S. Lienemann, J. Zötterman, S. Farnebo and K. Tybrandt, Stretchable gold nanowire-based cuff electrodes for low-voltage peripheral nerve stimulation, *J. Neural Eng.*, 2021, **18**, 045007.
- S. B. Yang, B.-S. Kong, D.-H. Jung, Y.-K. Baek, C.-S. Han, S.-K. Oh and H.-T. Jung, Recent advances in hybrids of carbon



- nanotube network films and nanomaterials for their potential applications as transparent conducting films, *Nanoscale*, 2011, **3**, 1361-1373.
32. X. Lu, Y. Zhang and Z. Zheng, Metal-Based Flexible Transparent Electrodes: Challenges and Recent Advances, *Adv. Electron. Mater.*, 2021, **7**, 2001121.
33. M. Bianchi, S. Guzzo, A. Lunghi, P. Greco, A. Pisciotta, M. Murgia, G. Carnevale, L. Fadiga and F. Biscarini, Synergy of Nanotopography and Electrical Conductivity of PEDOT/PSS for Enhanced Neuronal Development, *ACS Appl. Mater. Interfaces*, 2023, **15**, 59224-59235.
34. K. Gmucová, Fundamental aspects of organic conductive polymers as electrodes, *Curr. Opin. Electrochem.*, 2022, **36**, 101117.
35. J. Chen, C. Ye, T. Cang, R. Gao and X. Li, Recent advances in the construction and application of stretchable PEDOT smart electronic membranes, *J. Mater. Chem. C*, 2023, **11**, 14930-14967.
36. Y. Wang, C. Zhu, R. Pfattner, H. Yan, L. Jin, S. Chen, F. Molina-Lopez, F. Lissel, J. Liu, N. I. Rabiah, Z. Chen, J. W. Chung, C. Linder, M. F. Toney, B. Murmann and Z. Bao, A highly stretchable, transparent, and conductive polymer, *Sci. Adv.*, 2017, **3**, e1602076.
37. J. Chen, R. Hou, S. Li, C. Sun, K. Peng, Y. Dai and X. Chen, PAM/CNTs-Au microcrack sensor with high sensitivity and wide detection range for multi-scale human motion detection, *Sens. Actuators A-Phys.*, 2024, **370**, 115203.
38. C. A. Silva, J. Lv, L. Yin, I. Jeerapan, G. Innocenzi, F. Soto, Y. G. Ha and J. Wang, Liquid Metal Based Island-Bridge Architectures for All Printed Stretchable Electrochemical Devices, *Adv. Funct. Mater.*, 2020, **30**, 2002041.
39. O. V. Khutoryanskaya, Z. A. Mayeva, G. A. Mun and V. V. Khutoryanskiy, Designing Temperature-Responsive Biocompatible Copolymers and Hydrogels Based on 2-Hydroxyethyl(meth)acrylates, *Biomacromolecules*, 2008, **9**, 3353-3361.
40. J. S. Vukovic, M. M. Babic, K. M. Antic, J. M. Filipovic, S. T. Stojanovic, S. J. Najman and S. L. Tomic, *In vitro* cytotoxicity assessment of intelligent acrylate based hydrogels with incorporated copper in wound management, *Mater. Chem. Phys.*, 2016, **175**, 158-163.
41. M. Seiti, A. Giuri, C. E. Corcione and E. Ferraris, Advancements in tailoring PEDOT: PSS properties for bioelectronic applications: A comprehensive review, *Biomater. Adv.*, 2023, **154**, 213655.
42. J. Cao, X. Yang, J. Rao, A. Mitriashkin, X. Fan, R. Chen, H. Cheng, X. Wang, J. Goh, H. L. Leo and J. Ouyang, Stretchable and Self-Adhesive PEDOT:PSS Blend with High Sweat Tolerance as Conformal Biopotential Dry Electrodes, *ACS Appl. Mater. Interfaces*, 2022, **14**, 39159-39171.
43. M. Luitz, M. Lunzer, M. Mader, F. Kotz-Helmer and B. E. Rapp, presented in part at the Microfluidics, BioMEMS, and Medical Microsystems XX, 2022.
44. A. M. Loye, H.-K. Kwon, D. Dellal, R. Ojeda, S. Lee, R. Davis, N. Nagle, P. G. Doukas, J. Schroers, F. Y. Lee and T. R. Kyriakides, Biocompatibility of platinum-based bulk metallic glass in orthopedic applications, *Biomed. Mater.*, 2021, **16**, 045018.
45. J.-E. Park, H. S. Kang, M. Koo and C. Park, Autonomous Surface Reconciliation of a Liquid-Metal Conductor Micropatterned on a Deformable Hydrogel, *Adv. Mater.*, 2020, **32**, 2002178.
46. H. Cai, Z. Wang, N. W. Utomo, Y. Vidavsky and M. N. Silberstein, Highly stretchable ionically crosslinked acrylate elastomers inspired by polyelectrolyte complexes, *Soft Matter*, 2022, **18**, 7679-7688.
47. S. Chibani, C. Michel, F. Delbecq, C. Pinel and M. Besson, On the key role of hydroxyl groups in platinum-catalysed alcohol oxidation in aqueous medium, *Catal. Sci. Technol.*, 2013, **3**, 339-350.
48. S. Huang, Y. Liu, Y. Zhao, Z. Ren and C. F. Guo, Flexible Electronics: Stretchable Electrodes and Their Future, *Adv. Funct. Mater.*, 2019, **29**, 1805924.
49. Y. Zhao, S. Zhang, T. Yu, Y. Zhang, G. Ye, H. Cui, C. He, W. Jiang, Y. Zhai, C. Lu, X. Gu and N. Liu, Ultra-conformal skin electrodes with synergistically enhanced conductivity for long-time and low-motion artifact epidermal electrophysiology, *Nat. Commun.*, 2021, **12**, 4880.
50. M. Sasaki, B. C. Karikkineth, K. Nagamine, H. Kaji, K. Torimitsu and M. Nishizawa, Highly Conductive Stretchable and Biocompatible Electrode-Hydrogel Hybrids for Advanced Tissue Engineering, *Adv. Healthc. Mater.*, 2014, **3**, 1919-1927.
51. H. Yabu, K. Nagamine, J. Kamei, Y. Saito, T. Okabe, T. Shimazaki and M. Nishizawa, Stretchable, transparent and molecular permeable honeycomb electrodes and their hydrogel hybrids prepared by the breath figure method and sputtering of metals, *RSC Adv.*, 2015, **5**, 88414-88418.
52. B. Guo, Y. Zhong, X. Chen, S. Yu and J. Bai, 3D printing of electrically conductive and degradable hydrogel for epidermal strain sensor, *Compos. Commun.*, 2023, **37**, 101454.
53. J. Lee, D. Lee, D. Lim and K. Yang, Structural, electrical and optical properties of ZnO:Al films deposited on flexible organic substrates for solar cell applications, *Thin Solid Films*, 2007, **515**, 6094-6098.
54. C. Lim, Y. Shin, J. Jung, J. H. Kim, S. Lee and D.-H. Kim, Stretchable conductive nanocomposite based on alginate hydrogel and silver nanowires for wearable electronics, *APL Mater.*, 2018, **7**, 031502.
55. I. Kim, K. Woo, Z. Zhong, P. Ko, Y. Jang, M. Jung, J. Jo, S. Kwon, S.-H. Lee, S. Lee, H. Youn and J. Moon, A photonic sintering derived Ag flake/nanoparticle-based highly sensitive stretchable strain sensor for human motion monitoring, *Nanoscale*, 2018, **10**, 7890-7897.
56. Z. T. Tan, H. W. Li, Z. K. Niu, X. S. Chen, H. Yang, W. B. Lv, D. Y. Ji, J. Li, L. Q. Li and W. P. Hu, Armadillo-inspired micro-foldable metal electrodes with a negligible resistance change under large stretchability, *J. Mater. Chem. C*, 2021, **9**, 4046-4052.
57. L. Zhang, K. S. Kumar, H. He, C. J. Cai, X. He, H. Gao, S. Yue, C. Li, R. C.-S. Seet, H. Ren and J. Ouyang, Fully organic compliant dry electrodes self-adhesive to skin for long-term motion-robust epidermal biopotential monitoring, *Nat. Commun.*, 2020, **11**, 4683.
58. G. Li, K. Huang, J. Deng, M. Guo, M. Cai, Y. Zhang and C. F. Guo, Highly Conducting and Stretchable Double-Network Hydrogel for Soft Bioelectronics, *Adv. Mater.*, 2022, **34**, 2200261.
59. J. F. Moulder and J. Chastain, *Handbook of X-ray Photoelectron Spectroscopy: A Reference Book of Standard Spectra for Identification and Interpretation of XPS Data*, Physical Electronics Division, Perkin-Elmer Corporation, 1992.



60. S. Sharma and M. S. Hegde, Pt metal-CeO₂ interaction: Direct observation of redox coupling between Pt/Pt²⁺/Pt⁴⁺ and Ce⁴⁺/Ce³⁺ states in Ce_{0.98}Pt_{0.02}O_{2-δ} catalyst by a combined electrochemical and x-ray photoelectron spectroscopy study, *The Journal of Chemical Physics*, 2009, **130**, 114706.
61. N. Jiang, B. Huang, M. Wang, Y. Chen, Q. Yu and L. Guan, Universal and Energy-Efficient Approach to Synthesize Pt-Rare Earth Metal Alloys for Proton Exchange Membrane Fuel Cell, *Advanced Science*, 2024, **11**, 2305110.
62. J. S. Hammond and N. Winograd, XPS spectroscopic study of potentiostatic and galvanostatic oxidation of Pt electrodes in H₂SO₄ and HClO₄, *Journal of Electroanalytical Chemistry and Interfacial Electrochemistry*, 1977, **78**, 55-69.
63. M. A. Shah, Growth of uniform nanoparticles of platinum by an economical approach at relatively low temperature, *Scientia Iranica*, 2012, **19**, 964-966.
64. S. Azam, S. Munshi, M. K. Hassan and A. Fragoso, Temperature-Dependent Sheet Resistance and Surface Characterization of Thin Copper Films Bonded to FR4 Composite under Mechanical Vibrations, *Appl. Sci.*, 2023, **13**, 7941.
65. M. Reveil, V. C. Sorg, E. R. Cheng, T. Ezzyat, P. Clancy and M. O. Thompson, Finite element and analytical solutions for van der Pauw and four-point probe correction factors when multiple non-ideal measurement conditions coexist, *Rev. Sci. Instrum.*, 2017, **88**, 094704.
66. M. Ohring, in *Engineering Materials Science*, ed. M. Ohring, Academic Press, San Diego, 1995, pp. 559-610.
67. L. Wen, Y. Shi, J. Chen, B. Yan and F. Li, Wavy structures for stretchable energy storage devices: Structural design and implementation*, *Chin. Phys. B*, 2016, **25**, 018207.
68. K. Tybrandt, D. Khodagholy, B. Dielacher, F. Stauffer, A. F. Renz, G. Buzsáki and J. Vörös, High-Density Stretchable Electrode Grids for Chronic Neural Recording, *Adv. Mater.*, 2018, **30**, 1706520.
69. M. N. Gueye, A. Carella, J. Faure-Vincent, R. Demadrille and J.-P. Simonato, Progress in understanding structure and transport properties of PEDOT-based materials: A critical review, *Prog. Mater. Sci.*, 2020, **108**, 100616.
70. B. e. Zhu, H. Zhou, Y. Li, X. Wang and K. Xu, Recent Advances in Laser-Induced Phase Separation of PEDOT:PSS for Bioelectronics, *Advanced Photonics Research*, 2025, **6**, 2500104.
71. H. Zhou, Z. Jin, Y. Xu, Y. Lu, Z. Xia, F. Yang, Q. Wu, Y. Gao, J. Yin, J. Zhang, C. Ni, B. Zhang, Y. He, H. Yang and K. Xu, Enhanced laser-induced PEDOT-based hydrogels for highly conductive bioelectronics, *National Science Review*, 2025, **12**, nwaf136.
72. B. Cho, K. S. Park, J. Baek, H. S. Oh, Y.-E. Koo Lee and M. M. Sung, Single-Crystal Poly(3,4-ethylenedioxythiophene) Nanowires with Ultrahigh Conductivity, *Nano Letters*, 2014, **14**, 3321-3327.
73. H. Y. Jang, S.-K. Lee, S. H. Cho, J.-H. Ahn and S. Park, Fabrication of Metallic Nanomesh: Pt Nano-Mesh as a Proof of Concept for Stretchable and Transparent Electrodes, *Chem. Mater.*, 2013, **25**, 3535-3538.
74. H. Zhang, Y. Shao, R. Xia, G. Chen, X. Xiang and Y. Yu, Stretchable Electrodes with Interfacial Percolation Network, *Adv. Mater.*, 2024, **36**, 2401550.
75. G. V. Sreevanya, S.-J. Lee, H. Cheon, M. Kim and H.-K. Kim, Highly stretchable and flexible kirigami-patterned silver electrodes for wearable electronics, *Sens. Actuators A-Phys.*, 2024, **378**, 115813.
76. Y. Kim, S. Yoo and J.-H. Kim, Water-Based Highly Stretchable PEDOT:PSS/Nonionic WPU Transparent Electrode, *Polymers*, 2022, **14**, 949.
77. C. Lee, C. D. O'Connell, C. Onofrillo, P. F. M. Choong, C. Di Bella and S. Duchi, Human articular cartilage repair: Sources and detection of cytotoxicity and genotoxicity in photo-crosslinkable hydrogel bioscaffolds, *Stem Cells Transl. Med.*, 2020, **9**, 302-315.
78. X. Gao, Y. Bao, Z. Chen, J. Lu, T. Su, L. Zhang and J. Ouyang, Bioelectronic Applications of Intrinsically Conductive Polymers, *Adv. Electron. Mater.*, 2023, **9**, 2300082.
79. Z. Ma, Q. Huang, Q. Xu, Q. Zhuang, X. Zhao, Y. Yang, H. Qiu, Z. Yang, C. Wang, Y. Chai and Z. Zheng, Permeable superelastic liquid-metal fibre mat enables biocompatible and monolithic stretchable electronics, *Nat. Mater.*, 2021, **20**, 859-868.
80. J. E. Lim, D. Y. Lee and H. K. Kim, Mechanical Stretchability of Screen-Printed Ag Nanoparticles Electrodes on Polyurethane Substrate for Stretchable Interconnectors and Thin Film Heaters, *ECS J. Solid State Sci. Technol.*, 2018, **7**, 468-472.
81. S. Yoon, Y. J. Kim, Y. R. Lee, N.-E. Lee, Y. Won, S. Gandla, S. Kim and H.-K. Kim, Highly stretchable metal-polymer hybrid conductors for wearable and self-cleaning sensors, *NPG Asia Mater.*, 2021, **13**, 4.
82. J. Bang, J. Ahn, J. Zhang, T. H. Ko, B. Park, Y. M. Lee, B. K. Jung, S. Y. Lee, J. Ok, B. H. Kim, T.-i. Kim, J.-I. Choi, C. H. Lee and S. J. Oh, Stretchable and Directly Patternable Double-Layer Structure Electrodes with Complete Coverage, *ACS Nano*, 2022, **16**, 12134-12144.
83. Y. J. Fan, P. T. Yu, F. Liang, X. Li, H. Y. Li, L. Liu, J. W. Cao, X. J. Zhao, Z. L. Wang and G. Zhu, Highly conductive, stretchable, and breathable epidermal electrode based on hierarchically interactive nano-network, *Nanoscale*, 2020, **12**, 16053-16062.
84. D. Wu, S. Wu, P. Narongdej, S. Duan, C. Chen, Y. Yan, Z. Liu, W. Hong, I. Frenkel and X. He, Fast and Facile Liquid Metal Printing via Projection Lithography for Highly Stretchable Electronic Circuits, *Adv. Mater.*, 2024, **36**, 2307632.
85. K. R. Park, K.-b. Jang, S. Kim, D.-w. Han, J. H. Park, S. Y. Kim, K.-M. Kim, S. Yoo and S. Mhin, Design of Ag/PDMS electrodes with a pillar structure for stretchable electronics, *Microelectron. Eng.*, 2022, **265**, 111873.
86. D. Wu, B. Yao, S. Wu, H. Hingorani, Q. Cui, M. Hua, I. Frenkel, Y. Du, T. K. Hsiai and X. He, Room-Temperature Annealing-Free Gold Printing via Anion-Assisted Photochemical Deposition, *Adv. Mater.*, 2022, **34**, 2201772.
87. J. Liang, K. Tong and Q. Pei, A Water-Based Silver-Nanowire Screen-Print Ink for the Fabrication of Stretchable Conductors and Wearable Thin-Film Transistors, *Adv. Mater.*, 2016, **28**, 5986-5996.
88. W. Zu, Y. Ohm, M. R. Carneiro, M. Vinciguerra, M. Tavakoli and C. Majidi, A Comparative Study of Silver Microflakes in Digitally Printable Liquid Metal Embedded Elastomer Inks for Stretchable Electronics, *Adv. Mater. Technol.*, 2022, **7**, 2200534.



89. Y.-G. Park, H. Min, H. Kim, A. Zhexembekova, C. Y. Lee and J.-U. Park, Three-Dimensional, High-Resolution Printing of Carbon Nanotube/Liquid Metal Composites with Mechanical and Electrical Reinforcement, *Nano Letters*, 2019, **19**, 4866-4872.
90. C. Lim, S. Lee, H. Kang, Y. S. Cho, D.-H. Yeom, S.-H. Sunwoo, C. Park, S. Nam, J. H. Kim, S.-P. Lee, D.-H. Kim and T. Hyeon, Highly Conductive and Stretchable Hydrogel Nanocomposite Using Whiskered Gold Nanosheets for Soft Bioelectronics, *Adv. Mater.*, 2024, **36**, 2407931.
91. S. Ahmed, M. Momin, J. Ren, H. Lee and T. Zhou, Self-Assembly Enabled Printable Asymmetric Self-Insulated Stretchable Conductor for Human Interface, *Adv. Mater.*, 2024, **36**, 2400082.
92. D. H. Lee, T. Lim, J. Pyeon, H. Park, S.-W. Lee, S. Lee, W. Kim, M. Kim, J.-C. Lee, D.-W. Kim, S. Han, H. Kim, S. Park and Y.-K. Choi, Self-Mixed Biphasic Liquid Metal Composite with Ultra-High Stretchability and Strain-Insensitivity for Neuromorphic Circuits, *Adv. Mater.*, 2024, **36**, 2310956.
93. S. Benedikt, J. Wang, M. Markovic, N. Moszner, K. Dietliker, A. Ovsianikov, H. Grützmacher and R. Liska, Highly efficient water-soluble visible light photoinitiators, *J. Polym. Sci. A Polym. Chem.*, 2016, **54**, 473-479.
94. J. Frontiñán-Rubio, M. V. Gómez, C. Martín, J. M. González-Domínguez, M. Durán-Prado and E. Vázquez, Differential effects of graphene materials on the metabolism and function of human skin cells, *Nanoscale*, 2018, **10**, 11604-11615.

View Article Online
DOI: 10.1039/D6QM00189K



Data Availability Statement

View Article Online
DOI: 10.1039/D6QM00189K

Data for this article, including raw data for surface resistance, mechanical properties, XPS, SEM are available at ZENODO at <https://doi.org/10.5281/zenodo.18940924>

